LAWRENCE
LIVERMORE
NATIONAL
LABORATORY

LLNL-JRNL-609719

An analysis of the short-term cloud feedback using MODIS data

C. Zhou, M. Zelinka, A. Dessler, P. Yang

January 7, 2013

Journal of Climate

Disclaimer

An analysis of the short-term cloud feedback using MODIS data

C. Zhou[1], M.D. Zelinka[2], A.E. Dessler[1], P. Yang[1]

[1] Dept. of Atmospheric Sciences
Texas A&M University
College Station, TX
979-862-1427

[2] Program for Climate Model Diagnosis and Intercomparison,
Lawrence Livermore National Laboratory, Livermore, California, USA

Corresponding author: adessler@tamu.edu

Abstract

The cloud feedback in response to short-term climate variations is estimated from cloud measurements combined with off-line radiative transfer calculations. The cloud measurements are made by the Moderate Resolution Imaging Spectroradiometer (MODIS) on NASA's Terra satellite and cover the period 2000-2010. Low clouds provide a strong negative cloud feedback, mainly due to their impact in the shortwave (SW) portion of the spectrum. Mid-level clouds provide a positive net cloud feedback that is a combination of a positive SW feedback partially canceled by a negative feedback in the longwave (LW). High clouds have only a small impact on the net cloud feedback due to a close cancellation between large LW and SW cloud feedbacks. Segregating the clouds by optical depth, we find that the net cloud feedback is set by a positive cloud feedback due to reductions in the thickest clouds (mainly in the SW) and a cancelling negative feedback from increases in clouds with moderate optical depths (also mainly in the SW). The global average SW, LW, and net cloud feedbacks are +0.30±1.10, -0.46±0.74, and -0.16±0.83 $W/m^2/K$, respectively. The SW feedback is consistent with previous work; the MODIS LW feedback is lower than previous calculations and there are reasons to suspect it may be biased low. Finally, it is shown that the apparently small control that global mean surface temperature exerts on clouds, which leads to the large uncertainty in the short-term cloud feedback, arises from statistically significant but offsetting relationships between individual cloud types and global mean surface temperature.

35 **1. Introduction**

36 Clouds cover about two thirds of the Earth's surface and substantially regulate the Earth's
37 radiation budget. They cool the planet by reflecting shortwave (SW, 0.2-4 μm) radiation back
38 to space, and warm it by reducing outgoing longwave (LW, > 4.54 μm) radiation. In our
39 present climate, the SW effect dominates, so the net effect of clouds is to cool the planet (e.g.,
40 Allan, 2011). As the climate warms, however, the effect of clouds on the planet's radiation
41 balance may also change, resulting in a feedback to the global climate system. Uncertainty in
42 the magnitude of this cloud feedback is one of the primary contributors to the large spread of
43 climate sensitivity estimated by general circulation models (GCMs) (e.g., Dufresne and Bony,
44 2008). Therefore, improving our understanding of the cloud feedback is an important step for
45 improving our confidence in predictions of future climate change.

46 Many previous studies have examined the cloud feedback in GCMs in response to long-
47 term global warming (Colman, 2003; Soden and Held, 2006; Dessler, 2012), finding a cloud-
48 feedback magnitude ranging from near zero to > 1 $W/m^2/K$. There are, however, few
49 estimates from observations, mainly owing to the dearth of data of appropriate length and
50 quality. Dessler (2010; 2012) used measurements of top-of-atmosphere (TOA) flux from the
51 Clouds and the Earth's Radiant Energy System (CERES) and estimated that the cloud
52 feedback in response to short-term climate variations is positive and has a magnitude of
53 $\sim+0.5\pm0.8$ $W/m^2/K$.

54 Other studies have investigated regional cloud feedbacks in observations. Clement *et al.*
55 (2009) used a cloud dataset from the Northeast Pacific to show that low clouds in that region
56 acted as a positive feedback to multi-decadal regional surface temperature changes. The
57 GCMs that best reproduced the cloud behavior in that region and on that timescale had

58 average or stronger positive global cloud feedbacks in response to long-term global warming
59 (see also Broccoli and Klein, 2010). Zelinka and Hartmann (2011) showed that high tropical
60 clouds rose and contracted in area in response to interannual warming, leading to a net
61 positive short-term cloud feedback from these types of clouds, although the cloud anomalies
62 differed in subtle ways from those occurring under long-term warming (Zelinka and
63 Hartmann 2010).
64 In this study, direct satellite observations of cloud properties are used to further
65 investigate the details of the short-term cloud feedback, including comparisons to the cloud
66 feedback calculations of Dessler (2010; 2012). In addition to providing an independent
67 estimate of the short-term cloud feedback, this study is novel in that we will partition the
68 cloud feedback by cloud type. This allows us to clearly identify the role of robust but
69 opposing cloud changes in producing the net global cloud feedback. While it is unclear what
70 the short-term cloud feedback tells us about the cloud feedback in response to long-term
71 global warming (Dessler, 2010; 2012), the short-term cloud feedback nevertheless provides a
72 useful testbed for our theories of the cloud feedback and as a test of climate models.
73
74 **2. Data and methodology**
75 Our cloud feedback calculations use cloud observations made by the Moderate
76 Resolution Imaging Spectroradiometer (MODIS) onboard NASA's Terra satellite (Platnick *et*
77 *al.*, 2003). We analyze here monthly joint histograms of cloud-top pressure (P_{top}) and cloud
78 optical depth (τ) from the MOD08 product (Hubanks *et al.*, 2008) and covering the period
79 March 2000 to February 2010. Figure 1a plots the average cloud fraction over this period in
80 each P_{top}-τ bin. Integration over all bins yields a total cloud fraction of 48%.

To calculate the cloud feedback, we first calculate $\Delta R_{cloud}(lon,lat,P_{top},\tau)$, which is the contribution to the TOA flux anomaly from the cloud fraction anomaly at a particular latitude and longitude for clouds with a particular P_{top} and τ:

$$\Delta R_{cloud}(lon,lat,P_{top},\tau) = \frac{\partial R}{\partial C(P_{top},\tau)} \times \Delta C(lon,lat,P_{top},\tau), \quad (1)$$

where R is the TOA radiation flux and $\Delta C(\text{lon,lat},P_{top},\tau)$ is the cloud fraction anomaly. The MODIS data provide ΔC for every month, so using Eq. (1) we can produce a monthly time series of ΔR_{cloud}. All anomalies in this paper are calculated as the departure from the mean annual cycle computed over the entire time series.

The term $\partial R/\partial C(P_{top},\tau)$ is the change in TOA flux per unit change in the fraction of clouds with a specified P_{top} and τ. These so-called cloud radiative kernels have been calculated using a radiative transfer model by Zelinka *et al*. (2012a) and are updated for this study by replacing the GCM-mean temperature, water vapor, and ozone fields used as input to the radiation code with monthly-mean fields from the ERA-Interim Reanalysis over the Terra MODIS period (Dee *et al.*, 2011). The kernels are calculated separately for SW and LW fluxes, allowing us to additionally separate the cloud feedback into SW and LW components. The kernels are functions of P_{top}, τ, latitude, month; the SW kernels are also functions of clear-sky surface albedo. Before computing ΔR_{cloud}, at each latitude we map the SW kernels from surface-albedo space to longitude using monthly climatological surface albedo from the ERA-Interim Reanalysis.

To calculate the cloud feedback for these clouds, we regress the time series of $\Delta R_{cloud}(lon,lat,P_{top},\tau)$ against the monthly global average surface temperature anomaly ΔT_s

102 using an ordinary least-squares fit. The stated uncertainties in this paper are the 95%
103 confidence interval, calculated as twice the standard error of the slope of the fit.
104
105 **3. The short-term cloud feedback from MODIS data**
106 Figure 1b shows the slope of the linear regression of global average $\Delta C(P_{top},\tau)$ vs. ΔT_s in
107 each P_{top}-τ bin — this is the change in cloud fraction per degree increase in ΔT_s. The largest
108 positive changes (i.e., ΔC increasing with increasing ΔT_s) are found in the lowest height bin
109 (pressures > 800 hPa), with large negative changes in the bins above (800-680 hPa). Figure 2
110 shows the spatial distribution of the response in the 800-1000 and 680-800 hPa layers. The
111 dominant response of clouds in both layers to changes in ΔT_s occurs over the oceans. In the
112 800-1000 hPa layer, positive responses occur over wide areas of the oceanic subtropics and
113 mid-latitudes. In the 680-800 hPa layer, the dominant responses are more localized and
114 negative, and primarily located over the ocean to the west of N. and S. America and Australia.
115 Figures 1c, 1d, and 1e show the global average net, SW, and LW cloud feedbacks,
116 respectively, in each cloud-top pressure/optical depth bin. To obtain these values,
117 $\Delta R_{cloud}(lon,lat,P_{top},\tau)$ is first averaged over all latitudes and longitudes, and then the global
118 average $\Delta R_{cloud}(P_{top},\tau)$ is regressed against ΔT_s to obtain the cloud feedback in each P_{top}, τ bin.
119 All other average cloud feedbacks are calculated similarly, by first averaging ΔR_{cloud} and then
120 regressing that average against ΔT_s.
121 The global average cloud feedbacks are summarized in Table 1. As pointed out by
122 Dessler and Loeb (2012) and confirmed here, the choice of ΔT_s data set can have a significant
123 impact on the calculated cloud feedback. Aside from the MERRA, all of the calculations
124 produce slightly negative net feedbacks (although statistically indistinguishable from zero),

125 which arise from a combination of a positive SW feedback and a larger negative LW feedback.
126 The MERRA seems to be an outlier in this regard — it predicts both a negative SW and LW
127 feedback. It is unclear why the MERRA result stands out, although given the uncertainty in
128 the fits, it could just be a statistical fluctuation. Averaging all of the calculations together and
129 combining the uncertainties in quadrature, the SW, LW, and net cloud feedbacks are
130 +0.30±1.10, -0.46±0.74, and -0.16±0.83 $W/m^2/K$ (excluding the MERRA results yields values
131 of +0.42±1.13, -0.51±0.75, -0.10±0.84 $W/m^2/K$). All subsequent calculations in the paper,
132 including all of the figures, use the GISTEMP ΔT_s data set (Hansen *et al.*, 2010).
133 Also listed in Table 1 are cloud feedback values calculated using CERES measurements
134 (Dessler, 2012; Dessler and Loeb, 2012; Dessler, 2010). CERES measures the TOA net flux;
135 ΔR_{cloud} is calculated from those measurements by subtracting off the effects of changing water
136 vapor, surface and atmospheric temperature, surface albedo, and radiative forcing (Soden *et*
137 *al.*, 2008; Shell *et al.*, 2008). Thus, the CERES cloud feedback is derived not just from
138 different data, but from an entirely different method, so the comparison provides an important
139 test of the MODIS results.
140 The MODIS SW cloud feedback is 0.16-0.28 $W/m^2/K$ larger than the CERES SW cloud
141 feedbacks, which is a relatively small difference considering the uncertainty. We therefore
142 consider these quantities to be in good agreement. The MODIS LW cloud feedback is ~0.9
143 $W/m^2/K$ less than the CERES estimates, a much larger difference than for the SW feedback
144 estimates. Combining SW and LW feedbacks leads to the net cloud feedback from MODIS
145 observations ~0.7 $W/m^2/K$ lower than that from the CERES observations — a big enough
146 difference that the net feedback in the MODIS and CERES calculations have different signs.

147 To explore these differences in more detail, Figure 3 compares the SW, LW, and net
148 cloud feedback derived from MODIS and CERES as a function of latitude. The SW feedback
149 comparison reveals excellent agreement between the two data sets. In the LW, the cloud
150 feedback derived from CERES is more positive than the MODIS feedback at most latitudes.
151 Integrating over the globe, this small difference at each latitude sums to produce the large
152 underestimate of the global LW cloud feedback by MODIS discussed previously. In the net,
153 there is generally good agreement between the MODIS and CERES estimates. The largest
154 differences occur between 20°N and 60°N, where the CERES net cloud feedback is higher
155 than that from MODIS.

156 Thus, the main difference between these data sets is the lower LW cloud feedback from
157 MODIS. Some of the difference can be explained by the method: Zelinka *et al*. (2012a) found
158 that, in an analysis of GCMs, the cloud-kernel-derived LW cloud feedbacks were on average
159 0.15 $W/m^2/K$ lower than those computed using the method used to analyze the CERES data.

160 Limitations in the MODIS data may also contribute to the discrepancy. First, the optical
161 depths of thinner clouds ($\tau < 2$) are frequently not retrieved by MODIS (e.g., Marchand *et al.*,
162 2010). This includes about ~20% of the pixels identified as cloudy by the MODIS cloud
163 mask but for which the optical depth retrieval fails as well as clouds too thin to be flagged by
164 the cloud mask ($\tau \approx< 0.3$). This is reflected in Fig. 1a, which shows few clouds in the two
165 lowest τ bins (although other data show that clouds are indeed there (e.g, Dessler and Yang,
166 2003)). Second, MODIS optical depth is retrieved using a bispectral method involving both
167 visible and near-infrared bands (King *et al.*, 1992), so the MODIS data exclude nighttime
168 observations, including the wintertime high latitudes. Both of these issues will affect
169 MODIS's LW cloud feedback more than its SW feedback.

Another potential problem is an inconsistency between the MODIS retrieved cloud-top and the kernel. The kernel assumes the cloud top height is the height of the emitting level of the cloud (i.e., one optical depth into the cloud). However, the MODIS cloud-top is retrieved by a CO_2-slicing technique that retrieves a more accurate "edge" of the cloud, which tends to be higher than the emitting level of the cloud. This will also primarily affect the MODIS LW cloud feedback.

Yet another potential problem is a mismatch in the MODIS retrieval between cloud-top pressure and optical depth. For example, MODIS can correctly identify the cloud-top pressure of an optically thin high cloud over a thick lower cloud, but the retrieved optical thickness is for the whole column. This would produce the wrong LW ΔR_{cloud} when the retrieved properties of this cloud are multiplied by the LW cloud kernel (R. Pincus, personal communication, 2012), but would have much less of an effect on the SW ΔR_{cloud}.

The CERES-derived global average cloud feedbacks also have uncertainties. In addition to the uncertainty in the CERES measurements, the radiative kernels used to convert the CERES measurements to ΔR_{cloud} are derived from GCMs (Soden *et al.*, 2008; Shell *et al.*, 2008), so may not completely represent reality. Dessler and Loeb (2012) discuss the impact of different data sets on the CERES calculation.

Putting everything together, it is our judgment that the global-average cloud feedback from CERES is likely to be more reliable than the values obtained from the MODIS measurements. But even with potential global-average biases, the MODIS calculation is useful because it allows us to break the cloud feedback down by cloud type, something that cannot be done with the CERES data.

192 To further compare the MODIS and CERES cloud feedback calculations, Figure 4a and
193 4b show the spatial distribution of SW cloud feedback calculated from MODIS and CERES
194 observations. Regions that contribute positively (negatively) to the cloud feedback are colored
195 red (blue). The El Nino/La Nina Southern Oscillation (ENSO) is the dominant factor for the
196 interannual climate variations over the period analyzed, and therefore the regional distribution
197 of cloud feedback reflects a characteristic dipole pattern in the tropical Pacific. The difference
198 between the MODIS and CERES cloud feedback estimates are in Fig. 4c. Clearly, the
199 MODIS results agree well with those of CERES, capturing both the broad features and the
200 detailed spatial structures of the cloud-induced TOA flux anomalies.
201 Figures 4d, 4e, and 4f show the same plots for the LW. The LW feedback is essentially a
202 mirror image of the SW feedback, a consequence of the prominent role of high cloud
203 anomalies in causing the radiative anomalies and their opposing SW and LW effects on
204 climate. As with the SW, the difference between CERES and MODIS estimates is small.
205 Figures 4g, 4h, and 4i show the same plots for the net cloud feedback. This agreement in
206 the net feedbacks is particularly notable since the net feedback is a small residual of two large
207 but oppositely signed terms. Small errors in either the LW or SW term would lead to large
208 errors in the net feedback — the lack of large errors increases our confidence in the cloud
209 feedback calculations. The point-by-point agreement also means that the differences in the
210 global average feedbacks arise from small but widely distributed biases between the two
211 calculations.
212 To investigate the breakdown of the cloud feedback by cloud property, Figure 5 shows
213 the cloud response and cloud feedback as a function of cloud-top pressure. Fig. 5a shows the

214 biggest cloud changes occur for P_{top} above (altitudes below) 800 hPa. This layer by itself
215 drives a net global cloud feedback of -1.08±0.58 W/m^2/K (Fig. 5b).
216 At pressures below (altitudes above) 800 hPa, changes in clouds produce a weakly
217 negative LW cloud feedback (Fig. 5d) and a strongly positive SW cloud feedback (Fig. 5c),
218 leading to a net positive feedback of +1.06±0.69 W/m^2/K (Fig. 5b). Thus, the net global cloud
219 feedback is set by a negative feedback due to clouds near the surface and a slightly smaller
220 positive feedback due to clouds in the rest of the troposphere. Individually, both feedbacks are
221 statistically significant, but the sum over the whole troposphere is not. We will discuss this
222 last point in more detail in Section 4.
223 The largest LW cloud feedbacks are found in the uppermost bin, covering cloud-top
224 pressures of 180-50 hPa. The LW feedback there is negative and it plays a dominant role in
225 producing the overall negative global LW cloud feedback. These same cloud changes
226 generate an almost equivalent but oppositely signed SW cloud feedback (Figs. 5c). The net
227 cloud feedback at these altitudes is therefore close to zero (Fig. 5b). Figure 10 and Table 1 of
228 Zelinka and Hartmann (2011) show a similar amount of cancellation between LW and SW
229 fluxes in the upper troposphere, although that study focused on the tropics. Loeb *et al*. (2012)
230 also found a negative LW and positive SW tropical cloud feedback response to ENSO.
231 Figure 6 shows the distribution of the cloud changes and the associated feedbacks in the
232 uppermost layer, and the response of these clouds is quite different from the response of low-
233 level clouds in Fig. 2. Upper-level clouds show a classic ENSO dipole response of cloud
234 fraction changes in the tropical Pacific, and the pattern corresponds closely to the water vapor
235 feedback (Fig. 2 of Dessler, 2012). It is also clear that the resulting LW and SW feedbacks

236 substantially cancel each other — not just in the global average, but also at individual grid
237 points.

238 Figure 5 also breaks down the cloud feedback at each altitude into contributions from
239 changing cloud fraction and optical depth (in each case holding the other property fixed),
240 calculated using methodology derived from Zelinka *et al*. (2012b). The plot shows that, at
241 most altitudes, the cloud feedback is primarily due to changes in cloud fraction; changes in
242 optical depth make a smaller, positive contribution, mainly in the SW.

243 Figure 7 shows the feedback as a function of cloud optical depth. The fraction of clouds
244 with $\tau > 23$ decreases with increasing ΔT_s, while the fraction of clouds with $\tau < 23$ increases
245 (Fig. 7a). The increase in thin clouds at the expense of thick clouds leads to offsetting SW
246 cloud feedbacks for these two groups — summing them produces a the net positive SW cloud
247 feedback. Figure 7 also breaks down the cloud feedback at each optical depth into
248 contributions from changing cloud fraction and cloud top height. Changes in cloud height
249 have little impact in the SW, so the SW cloud feedback is mainly from changing cloud
250 fraction.

251 In the LW (Fig. 7d), the feedback is negative for all optical depth bins. The figure shows
252 that this overall negative feedback arises from a general competition between changing cloud
253 fraction and cloud top height. For the thickest clouds, the reduction in cloud fraction
254 dominates over the increase in cloud top height, leading to a negative LW feedback. For
255 thinner clouds, a reduction in cloud top height dominates the increase in cloud fraction, which
256 also leads to a negative LW feedback.

257 The net cloud feedback comes from a positive cloud feedback from thick cloud changes
258 and a slightly bigger negative feedback from changes in thinner clouds (Fig. 7b). Changes in

259 the thinnest clouds contribute little to the net feedback, although, as mentioned previously,
260 this might be a consequence of MODIS's inability to retrieve cloud properties for these thin
261 clouds. Indeed, tropical mean LW cloud feedbacks computed in the same manner as in this
262 study but using ISCCP (which retrieves significantly more thin clouds than MODIS
263 (Marchand *et al.*, 2010)) are consistently less negative than those computed using MODIS,
264 despite the SW cloud feedbacks being the same (Zelinka and Hartmann, 2011).

265 Figure 8 shows the latitudinal distribution of the cloud feedback broken down into high
266 ($P_{top} < 440$ hPa), mid-level ($440 < P_{top} < 680$ hPa) and low ($P_{top} > 680$ hPa) clouds. At most
267 latitudes, the biggest component of the LW or SW cloud feedback is from high clouds. The
268 LW and SW feedbacks of high clouds nearly cancel, however. This leads to a substantially
269 smaller net high-cloud feedback that is comparable at most latitudes to the net feedback from
270 mid-level and low clouds.

271 The latitudinal pattern of the high cloud feedbacks primarily reflects the equatorward
272 shift of the subtropical jets during the (warmer) El Nino phase of ENSO (e.g., Trenberth and
273 Hurrell, 1994). This moves cloudy regions onto the Equator and the clear subtropics towards
274 the equator — and results in the hemispherically symmetric pattern in the Tropics evident in
275 Fig. 8a.

276 Table 1 lists the global average cloud feedbacks broken down by altitude. Because the
277 changes in high clouds are primarily driven by rearrangements in the atmospheric circulation,
278 a large positive cloud feedback at one latitude will tend to be cancelled in the global average
279 by a large negative cloud feedback at another latitude. The global average high-cloud
280 feedbacks are therefore a small residual of these large and offsetting feedbacks from different
281 latitudes.

For lower clouds, the SW cloud feedback dominates and it is what mainly determines the net cloud feedback. For mid-level clouds, the net feedback is positive at most latitudes, leading to a positive global average. While the SW and net mid-level cloud feedback is smaller at most latitudes than the low- or high-cloud counterparts, it is also rarely negative. It therefore ends up being the largest positive contributor to the global mean feedback — and is the only component that is distinguishable from zero. For low clouds, averaging over the globe produces a strong negative SW and net cloud feedback.

Overall, the global SW cloud feedback is set by a positive feedback from mid-level and high clouds, which is reduced by about 50% by a negative feedback from low clouds. The global LW feedback is negative at all altitudes, with the greatest contribution coming from high clouds. The net cloud feedback is set by a negative feedback from low clouds that is almost entirely cancelled by positive cloud feedbacks from mid-level and high clouds.

Table 1 also lists a breakdown by optical depth. Viewed this way, the positive SW cloud feedback is set by a positive feedback from thick clouds that is partially cancelled by a negative feedback from mid-thickness and thin clouds. The negative LW cloud feedback is set primarily by thick clouds, with a smaller contribution from mid-thickness clouds. The net feedback is set by a positive feedback from thick clouds that is nearly cancelled by a negative feedback from mid-thickness and thin clouds.

4. Why is the cloud feedback so uncertain?

Dessler (2010; 2012) presented scatterplots of ΔR_{cloud}, the cloud-induced TOA flux anomaly, against ΔT_s, the global average surface temperature anomaly. The MODIS ΔR_{cloud} vs. GISTEMP ΔT_s plot is shown in Fig. 9a (slope = -0.02±0.76 W/m^2/K). The correlation

between these variables is poor and the scatter in the data results in a highly uncertain cloud feedback. One might conclude from this that clouds are only weakly impacted by ΔT_s variations.

Analysis of the MODIS data helps us refine our understanding of this issue. Figure 9b shows a scatterplot of ΔR_{cloud} vs. ΔT_s for the lowest layer (1000-800 hPa) (slope = -1.08±0.58 W/m^2/K) and Fig. 9c shows the same thing for the rest of the troposphere (800-50 hPa) (slope = +1.06±0.69 W/m^2/K). Both relations are statistically significant (although there is still considerable scatter), so one can conclude that clouds in these layers are indeed related to ΔT_s. The relationships have opposite signs, however, so when one considers the entire troposphere (Fig. 9a), they cancel and no clear relation exists.

This can also be seen in Fig. 1b-1e, in which P_{top}-τ bins that show statistically significant correlations with ΔT_s (at the 2σ level) are marked with a cross. About 40-50% of the bins show statistically significant relations (more than the 5% that would be expected due to chance), confirming in more detail the results in Fig. 9.

This reflects a general truth about these data: *the global average cloud feedback is a small residual of the sum of larger and often statistically significant quantities that oppose each other horizontally, vertically, in optical depth space, and spectrally (LW vs. SW)*. Thus, it is not correct to conclude, on the basis of a plot like Fig. 9a, that ΔT_s has little influence on clouds. Rather, individual cloud populations may indeed be controlled by ΔT_s, but cancellations in the global average calculations obscure the relationships.

Much of this cancellation may be due to the fact that most of the climate variation we are using to extract the cloud feedback comes from ENSO, which is a large-scale rearrangement of the atmospheric circulation. This rearrangement leads to large but compensating changes

328 in clouds, and therefore to the cancellation identified above. GCM simulations of long-term
329 global warming show a more uniform response, with both the LW and SW feedback being
330 positive at most latitudes (e.g., Dessler, 2012, Fig. 6; Zelinka *et al.*, 2012a, Fig. 6).
331
332 **5. Discussion and Conclusions**
333 In this study, MODIS observations of clouds are used to estimate the cloud feedback in
334 response to short-term climate variations. The global average net cloud feedback estimated
335 from MODIS is slightly negative — it arises by the near-balance between a negative LW
336 cloud feedback and a positive SW cloud feedback (Table 1).
337 These results have been compared to independent estimates of the cloud feedback derived
338 from CERES TOA flux observations (Dessler, 2010; 2012). In the SW, the calculations show
339 good agreement and both predict a positive SW cloud feedback. In the LW, however, there
340 are significant differences: the MODIS LW feedback is negative, while that from CERES is
341 positive. Considering all potential sources of error, we judged that the more reliable global
342 average cloud feedback values are the ones obtained from the CERES data.
343 In response to short-term climate variations, the MODIS data show a strong increase in
344 low clouds (cloud-top pressures above (altitudes below) 800 hPa) as the climate warms (Fig.
345 5a), primarily occurring over oceans in the subtropics and midlatitudes (Fig. 2a). These cloud
346 changes produce a strong negative cloud feedback, almost entirely from increased SW
347 reflection. A concomitant decrease in clouds between 800 and 500 hPa yields a nearly
348 offsetting positive feedback, also predominantly in the SW (Fig. 5). Changes in high clouds
349 have significant SW and LW cloud feedbacks that nearly cancel, leading to little contribution

350 to the global net cloud feedback (Figs. 5b and 6). Thus, the majority of the net cloud feedback
351 comes from the lower troposphere.

352 Analyzing the cloud feedback as a function of optical depth (Fig. 7), the data show a
353 general decrease of τ as ΔT_s increases. The general thinning of clouds produces a positive
354 cloud feedback in the SW and a negative feedback in the LW.

355 Our results show that high clouds dominate the LW and SW cloud feedbacks at most
356 latitudes (Fig. 8). There is significant latitude-to-latitude variation in the magnitude and sign
357 of these quantities, so that the global average (Table 1) is a small residual of the large and
358 offsetting feedbacks at different latitudes.

359 Lower clouds experience less cancellation between their SW and LW components. Thus,
360 at any particular latitude, clouds at all levels play important roles in the net cloud feedback.
361 Integrating globally, Table 1 shows that the net cloud feedback is primarily determined by low
362 clouds, with mid-level clouds making a smaller contribution, and high clouds making an even
363 smaller contribution. Alternatively, one could view the net cloud feedback as being set by a
364 negative cloud feedback from low clouds in the SW and mid-level and high clouds in the LW,
365 which is almost entirely cancelled by a positive cloud feedback from mid-level and high
366 clouds in the SW.

367 We also discussed the scatter in the relation between ΔR_{cloud} and ΔT_s (Fig. 9a), which
368 leads to large uncertainty in the inferred cloud feedback. The scatter arises mainly because
369 ΔR_{cloud} is a small residual of larger, oppositely signed terms that in many cases are themselves
370 statistically significant. Small differences in either of the large terms — whether due to errors
371 in the measurement or calculation or to the fact that clouds are weakly affected by factors

372 other than ΔT_s — will lead to relatively large changes in ΔR_{cloud}. This produces the scatter in
373 the ΔR_{cloud} vs. ΔT_s relation and to the intrinsic uncertainty in estimates of the cloud feedback.
374 That this work is an analysis of the cloud response to short-term climate variations is an
375 important caveat. Previous work has shown little correlation between the cloud feedback in
376 response to these short-term (mainly ENSO) climate variations and the response to long-term
377 global warming (Dessler, 2010; Colman and Power, 2010; Dessler, 2012). Thus, the
378 implications of this for long-term global warming are unclear.
379
380 Acknowledgments: This work was supported by NSF grant AGS-1012665 to Texas A&M
381 University. CZ acknowledges support from NASA Earth and Space Science Fellowship grant
382 NNX12AN57H to Texas A&M University. The contribution of MDZ was performed under
383 the auspices of U.S. Department of Energy by Lawrence Livermore National Laboratory
384 (LLNL) under Contract DE-AC52-07NA27344 and was supported by the Regional and
385 Global Climate Modeling Program of the Office of Science at the U. S. Department of
386 Energy.
387
388

389 **References**

390 Allan, R. P., 2011: Combining satellite data and models to estimate cloud radiative effect at
391 the surface and in the atmosphere, Meteorological Applications, 18, doi:10.1002/met.285,
392 324-333.
393 Broccoli, A. J., and S. A. Klein, 2010: Comment on "Observational and Model Evidence for
394 Positive Low-Level Cloud Feedback", Science, 329, doi:10.1126/science.1186796.
395 Clement, A. C., R. Burgman, and J. R. Norris, 2009: Observational and Model Evidence for
396 Positive Low-Level Cloud Feedback, Science, 325, doi:10.1126/Science.1171255, 460-
397 464.
398 Colman, R., 2003: A comparison of climate feedbacks in general circulation models, Climate
399 Dynamics, 20, 865-873.
400 Colman, R. A., and S. B. Power, 2010: Atmospheric radiative feedbacks associated with
401 transient climate change and climate variability, Climate Dynamics, 34,
402 doi:10.1007/s00382-009-0541-8, 919-933.
403 Dee, D. P., et al., 2011: The ERA-Interim reanalysis: Configuration and performance of the
404 data assimilation system, Q. J. R. Meteor. Soc., 137, doi:10.1002/qj.828, 553-597.
405 Dessler, A. E., 2010: A determination of the cloud feedback from climate variations over the
406 past decade, Science, 330, doi:10.1126/science.1192546, 1523-1527.
407 Dessler, A. E., 2012: Observations of climate feedbacks over 2000-2010 and comparisons to
408 climate models, J. Climate, in press.
409 Dessler, A. E., and P. Yang, 2003: The distribution of tropical thin cirrus clouds inferred from
410 Terra MODIS data, J. Climate, 16, 1241-1248.
411 Dessler, A. E., and N. G. Loeb, 2012: Impact of dataset choice on calculations of the short-
412 term cloud feedback, J. Geophys. Res., submitted.
413 Dufresne, J. L., and S. Bony, 2008: An assessment of the primary sources of spread of global
414 warming estimates from coupled atmosphere-ocean models, J. Climate, 21,
415 doi:10.1175/2008jcli2239.1, 5135-5144.
416 Hansen, J., R. Ruedy, M. Sato, and K. Lo, 2010: Global surface temperature change, Rev.
417 Geophys., 48, Rg4004, doi:10.1029/2010rg000345.
418 Hubanks, P. A., M. D. King, S. Platnick, and R. Pincus (2008), MODIS Atmosphere L3
419 gridded product algorithm theoretical basis document, Rep. ATBD-MOD-30.

King, M. D., Y. J. Kaufman, W. P. Menzel, and D. Tanre, 1992: Remote sensing of cloud, aerosol, and water vapor properties from the Moderate Resolution Imaging Spectrometer (MODIS), Ieee Trans. Geosci. Remote, 30, 2-27.

Loeb, N. G., S. Kato, W. Su, T. Wong, F. Rose, D. R. Doelling, J. R. Norris, and X. Huang, 2012: Advances in understanding top-of-atmosphere radiation variability from satellite observations, Surveys in Geophysics, 33, doi:10.1007/s10712-012-9175-1, 359-385.

Marchand, R., T. Ackerman, M. Smyth, and W. B. Rossow, 2010: A review of cloud top height and optical depth histograms from MISR, ISCCP, and MODIS, J. Geophys. Res., 115, D16206, doi:10.1029/2009jd013422.

Morice, C. P., J. J. Kennedy, N. A. Rayner, and P. D. Jones, 2012: Quantifying uncertainties in global and regional temperature change using an ensemble of observational estimates: The HadCRUT4 data set, J. Geophys. Res., 117, D08101, doi:10.1029/2011jd017187.

Platnick, S., M. D. King, A. S. Ackerman, W. P. Menzel, B. A. Baum, J. C. Riedi, and R. A. Frey, 2003: The MODIS cloud products: Algorithms and examples from Terra, Ieee Trans. Geosci. Remote, 41, 459-473.

Rienecker, M. M., et al., 2011: MERRA - NASA's Modern-Era Retrospective Analysis for Research and Applications, J. Climate, 24, doi:10.1175/JCLI-D-11-00015.1, 3624-3648.

Shell, K. M., J. T. Kiehl, and C. A. Shields, 2008: Using the radiative kernel technique to calculate climate feedbacks in NCAR's Community Atmospheric Model, J. Climate, 21, doi:10.1175/2007jcli2044.1, 2269-2282.

Smith, T. M., R. W. Reynolds, T. C. Peterson, and J. Lawrimore, 2008: Improvements to NOAA's historical merged land-ocean surface temperature analysis (1880-2006), J. Climate, 21, doi:10.1175/2007jcli2100.1, 2283-2296.

Soden, B. J., and I. M. Held, 2006: An assessment of climate feedbacks in coupled ocean-atmosphere models, J. Climate, 19, 3354-3360.

Soden, B. J., I. M. Held, R. Colman, K. M. Shell, J. T. Kiehl, and C. A. Shields, 2008: Quantifying climate feedbacks using radiative kernels, J. Climate, 21, 3504-3520.

Trenberth, K. E., and J. W. Hurrell, 1994: Decadal atmosphere-ocean variations in the Pacific, Climate Dynamics, 9, doi:10.1007/bf00204745, 303-319.

449 Zelinka, M. D., and D. L. Hartmann, 2011: The observed sensitivity of high clouds to mean
450 surface temperature anomalies in the tropics, J. Geophys. Res., 116, D23103,
451 doi:10.1029/2011jd016459.
452 Zelinka, M. D., S. A. Klein, and D. L. Hartmann, 2012a: Computing and partitioning cloud
453 feedbacks using cloud property histograms. Part I: Cloud radiative kernels, J. Climate, 25,
454 doi:10.1175/jcli-d-11-00248.1, 3715-3735.
455 Zelinka, M. D., S. A. Klein, and D. L. Hartmann, 2012b: Computing and partitioning cloud
456 feedbacks using cloud property histograms. Part II: Attribution to changes in cloud
457 amount, altitude, and optical depth, J. Climate, 25, doi:10.1175/jcli-d-11-00249.1, 3736-
458 3754.
459
460
461

462 **Table 1. Summary of global average cloud feedbacks**
463 All values have units of $W/m^2/K$; uncertainties are $\pm 2\sigma$
464

MODIS cloud feedback	SW	LW	Net (LW+SW)
ΔT_s data set*:			
GISTEMP	+0.47±1.02	-0.48±0.68	-0.02±0.76
HadCRUT4	+0.50±1.20	-0.53±0.80	-0.03±0.90
ERA-interim skin temperature	+0.35±1.01	-0.45±0.68	-0.10±0.76
NCDC	+0.35±1.25	-0.58±0.84	-0.23±0.94
MERRA skin temperature	-0.17±1.02	-0.28±0.69	-0.45±0.76
Average	+0.30±1.10	-0.46±0.74	-0.16±0.83
Average (excluding MERRA)	+0.42±1.13	-0.51±0.75	-0.10±0.84
CERES cloud feedback			
Average of values in Table 1 of Dessler and Loeb (2012) (Terra period)	+0.14±0.78	+0.43±0.47	+0.57±0.71
Breakdown by cloud altitude**			
Low ($P_{top} > 680$ hPa)	-0.46±0.68	-0.04±0.09	-0.50±0.61
Mid-level ($440 < P_{top} < 680$ hPa)	+0.50±0.36	-0.14±0.11	+0.35±0.28
High ($P_{top} < 440$ hPa)	+0.43±0.78	-0.30±0.71	+0.13±0.25
Breakdown by cloud optical depth**			
Thin ($\tau < 3.6$)	-0.22±0.14	+0.01±0.14	-0.21±0.13
Middle ($3.6 < \tau < 23$)	-0.31±0.76	-0.12±0.44	-0.43±0.56
Thick ($\tau > 23$)	+0.99±0.90	-0.37±0.38	+0.62±0.54

465 *Source of ΔT_s data: GISTEMP: Hansen et al. (2010); HadCRUT4: Morice et al. (2012);
466 ERA-interim: Dee et al. (2011); the National Climatic Data Center (NCDC): Smith et al.
467 (2008); NASA's Modern Era Retrospective-analysis for Research and Application (MERRA):
468 Rienecker et al. (2011);
469 **calculated using GISTEMP ΔT_s.
470

Figure captions

Figure 1. (a) Average cloud fraction in each P_{top}-τ bin (%). (b) Slope of the regression of cloud-fraction anomaly in each bin vs. ΔT_s (%/K). (c-e) The contribution to the net cloud feedback, SW cloud feedback, and LW cloud feedback, respectively, in W/m^2/K. Note that the multiplication of cloud radiative kernels with cloud fraction anomalies occurs at every location and is then spatially averaged for display in this figure. Bins where the regression slope is statistically significant (>95%) are marked with black crosses.

Figure 2. Change in cloud fraction per degree increase in global average ΔT_s (%/K) in (a) the 800-1000 hPa layer and (b) the 680-800 hPa layer. The y-axis in these plots is area-weighted latitude.

Figure 3. The zonal mean cloud feedbacks. The red line is the cloud feedback calculated from MODIS, and the red shading represents the 95% confidence range. The blue line is the feedback from CERES (Dessler, 2010; 2012), and the blue shading represents the 95% confidence range (where they overlap, the shading is purple).

Figure 4. Spatial distribution of the short-term cloud feedback (W/m2/K) calculated from MODIS observations (left panels) and CERES (middle panels) and the difference (MODIS minus CERES) (right panels). (a-c) are the SW component of cloud feedback, (d-f) are for LW cloud feedback, and (g-i) are for net cloud feedback. The CERES □Rcloud values are from Dessler [2010, 2012]. The y-axis in these plots is area-weighted latitude.

494

495 Figure 5. (a) Altitude profile of the change of global mean cloud fraction per degree of global
496 mean surface temperature anomaly (%/K). (b-d) The heavy line shows the contribution to the
497 net, SW, and LW cloud feedbacks, respectively. The error bars indicate the 95% confidence
498 interval. Also shown are the contributions to the cloud feedback at each altitude from changes
499 in τ and cloud fraction, holding all else fixed.

500

501 Figure 6. (a) Change in cloud fraction per degree increase in global average ΔT_s (%/K) for the
502 180-50 hPa layer. (b-d) The contribution of cloud changes in this layer to the net, SW, and
503 LW cloud feedbacks in $W/m^2/K$. The y-axis is area-weighted latitude.

504

505 Figure 7. (a) Slope of the regression of cloud fraction vs. ΔT_s (%/K), as a function of cloud
506 optical depth. (b-d) The heavy line shows the contribution to the net, SW, and LW cloud
507 feedbacks, respectively. The error bars indicate the 95% confidence interval. Also shown are
508 the contributions to the cloud feedback at each optical depth from changes in cloud top height
509 and cloud fraction, holding all else fixed.

510

511 Figure 8. The zonal mean (a) high, (b) mid-level, and (c) low cloud feedbacks. The black solid
512 line is the total cloud feedback calculated from MODIS. The lines marked with circles and
513 plus signs represent the SW and LW components of the feedback, respectively.

514

515 Figure 9. Scatter plot of global average ΔR_{cloud} vs. ΔT_s for (a) the entire troposphere (50-1000
516 hPa), (b) the 800-1000 hPa layer, and (c) the 50-800 hPa layer. The least-squares fit and the
517 2σ uncertainty of the fit are also plotted.
518
519

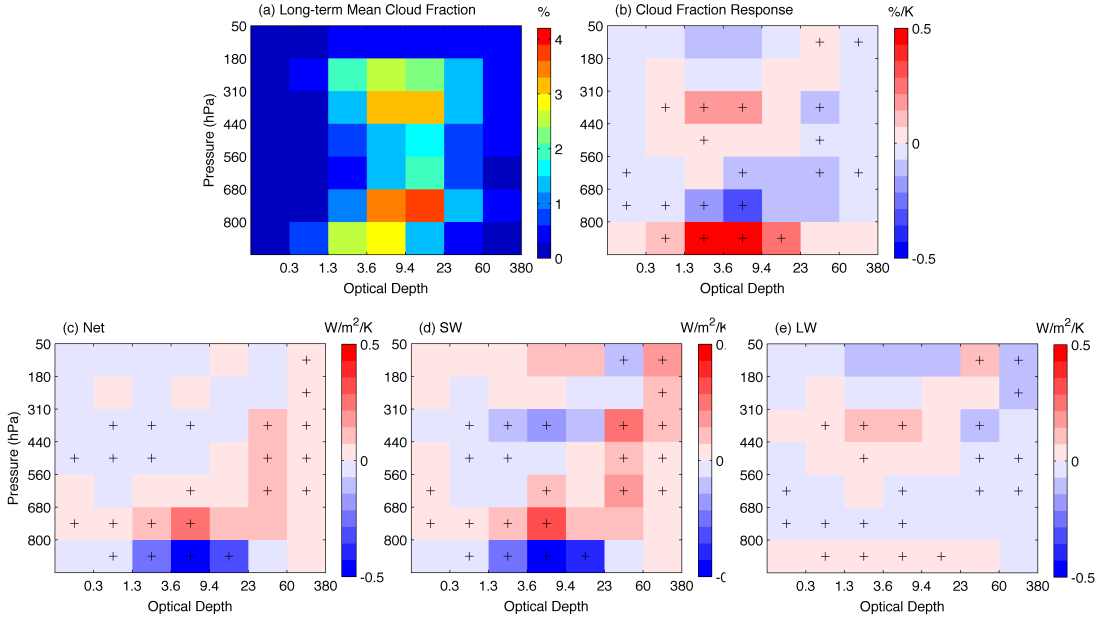

Figure 1. (a) Average cloud fraction in each P_{top}-τ bin (%). (b) Slope of the regression of cloud-fraction anomaly in each bin vs. ΔT_s (%/K). (c-e) The contribution to the net cloud feedback, SW cloud feedback, and LW cloud feedback, respectively, in W/m^2/K. Note that the multiplication of cloud radiative kernels with cloud fraction anomalies occurs at every location and is then spatially averaged for display in this figure. Bins where the regression slope is statistically significant (>95%) are marked with black crosses.

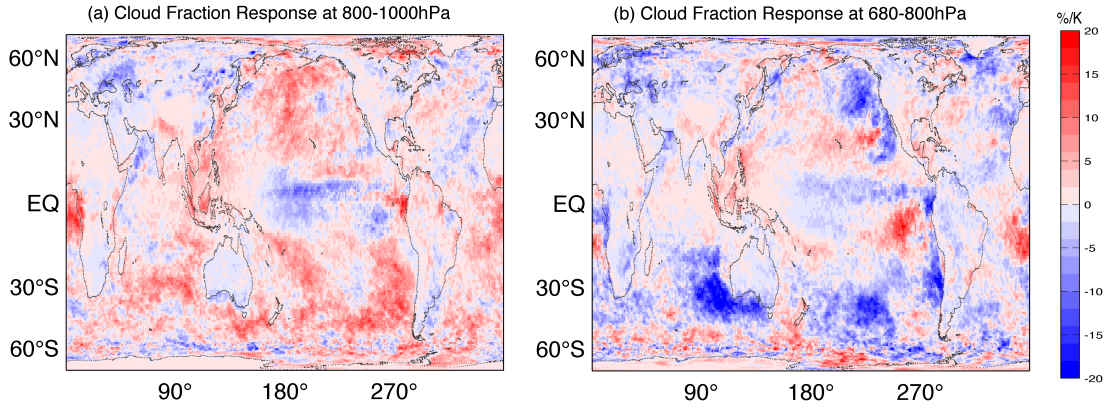

Figure 2. Change in cloud fraction per degree increase in global average ΔT_s (%/K) in (a) the 800-1000 hPa layer and (b) the 680-800 hPa layer. The y-axis in these plots is area-weighted latitude.

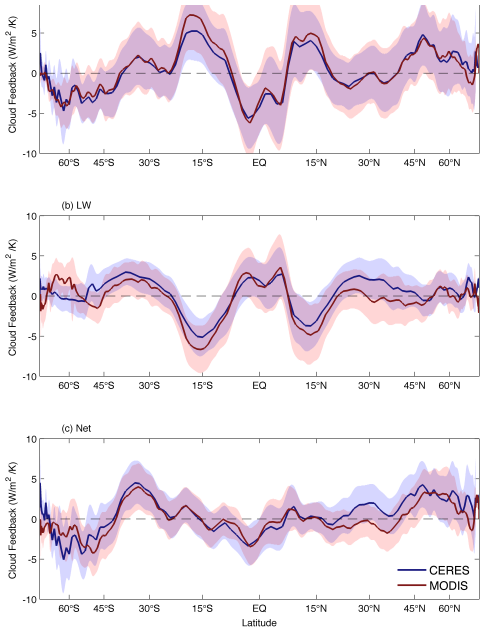

534
535 Figure 3. The zonal mean cloud feedbacks. The red line is the cloud feedback calculated from
536 MODIS, and the red shading represents the 95% confidence range. The blue line is the
537 feedback from CERES (Dessler, 2010; 2012), and the blue shading represents the 95%
538 confidence range (where they overlap, the shading is purple).

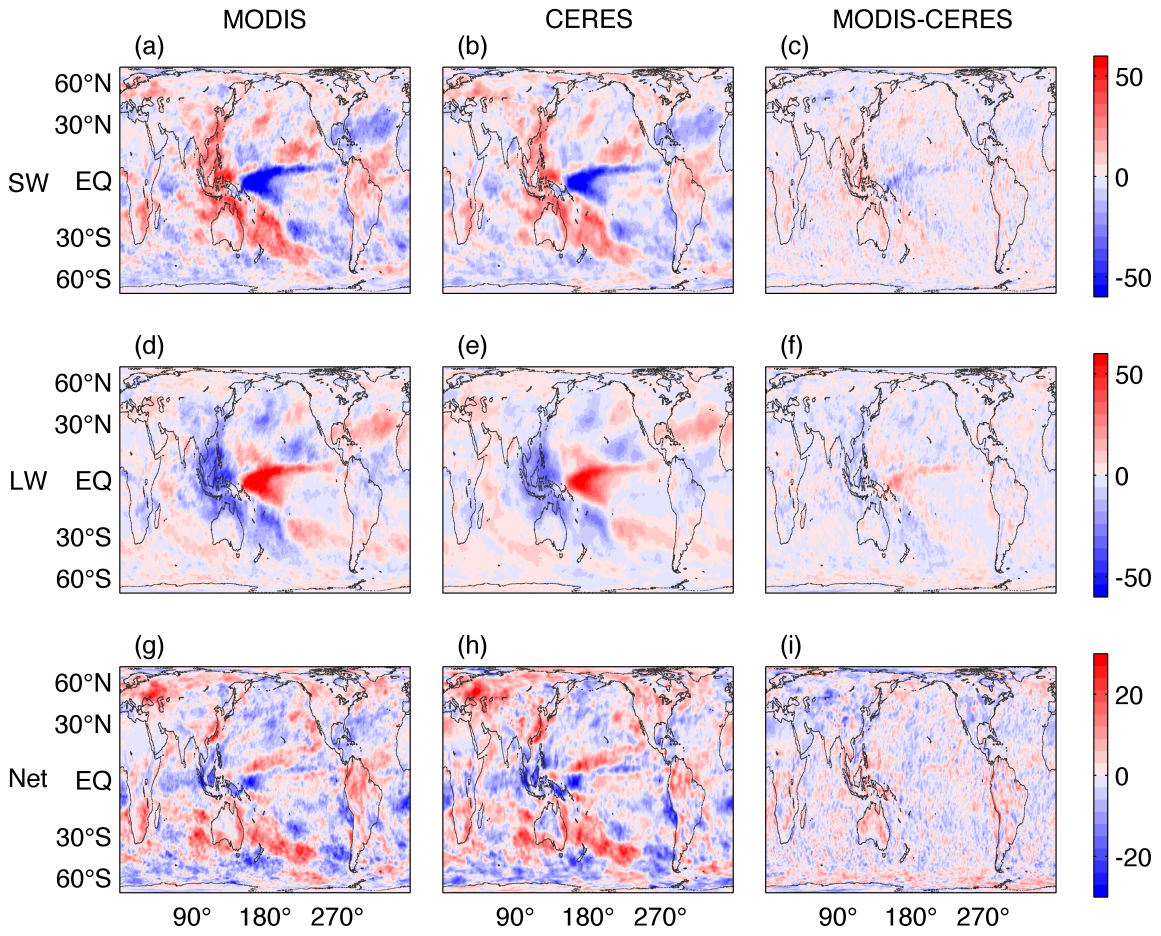

Figure 4. Spatial distribution of the short-term cloud feedback ($W/m^2/K$) calculated from MODIS observations (left panels) and CERES (middle panels) and the difference (MODIS minus CERES) (right panels). (a-c) are the SW component of cloud feedback, (d-f) are for LW cloud feedback, and (g-i) are for net cloud feedback. The CERES ΔR_{cloud} values are from Dessler [2010, 2012]. The y-axis in these plots is area-weighted latitude.

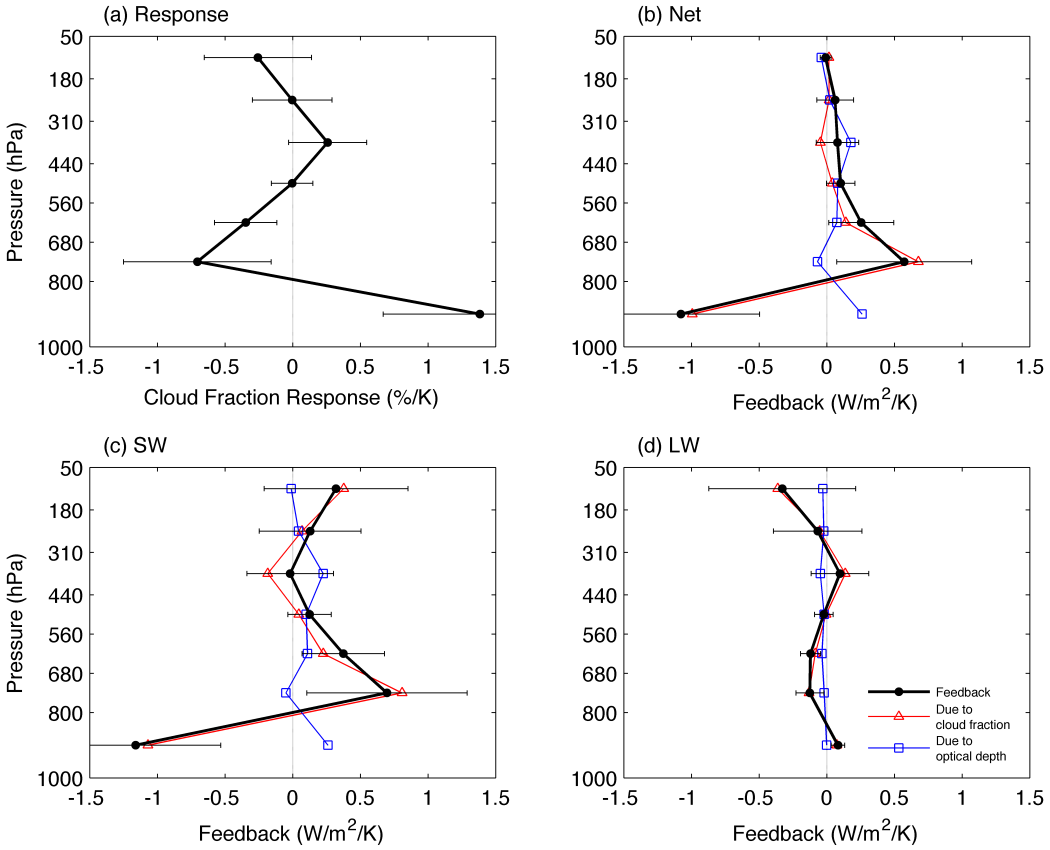

547 Figure 5. (a) Altitude profile of the change of global mean cloud fraction per degree of global
548 mean surface temperature anomaly (%/K). (b-d) The heavy line shows the contribution to the
549 net, SW, and LW cloud feedbacks, respectively. The error bars indicate the 95% confidence
550 interval. Also shown are the contributions to the cloud feedback at each altitude from changes
551 in τ and cloud fraction, holding all else fixed.

552

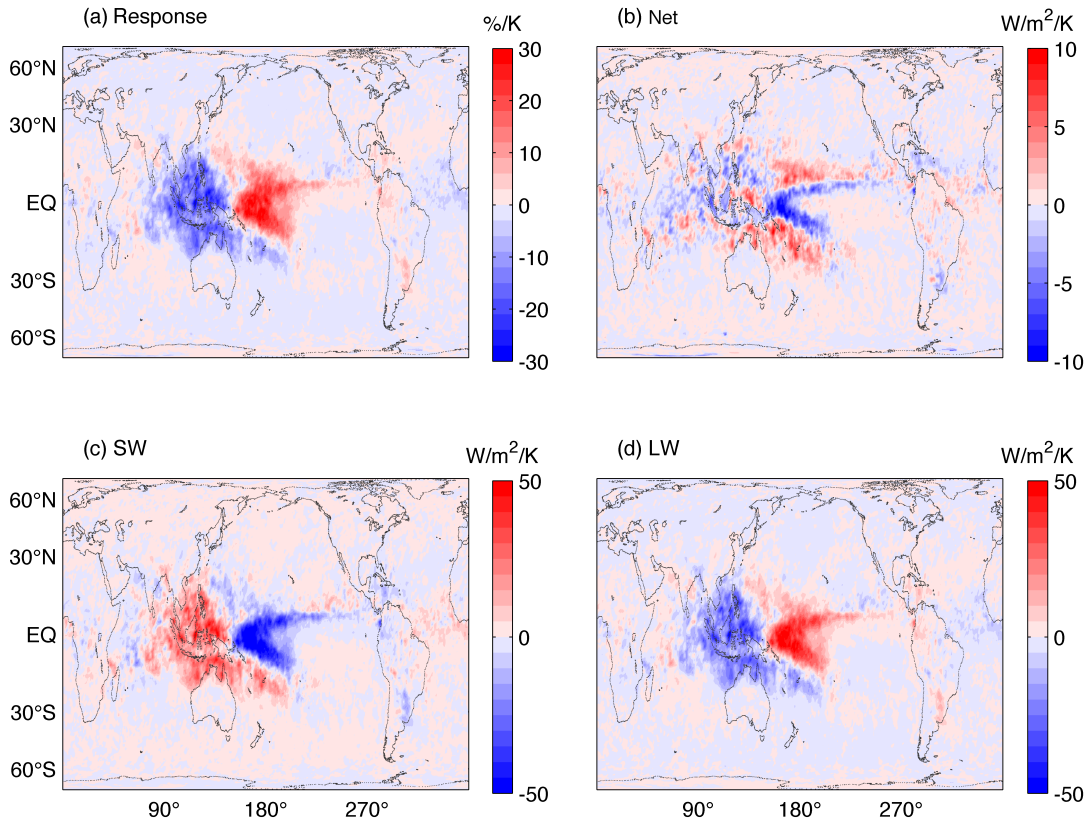

554 Figure 6. (a) Change in cloud fraction per degree increase in global average ΔT_s (%/K) for the
555 180-50 hPa layer. (b-d) The contribution of cloud changes in this layer to the net, SW, and
556 LW cloud feedbacks in W/m^2/K. The y-axis is area-weighted latitude.

557

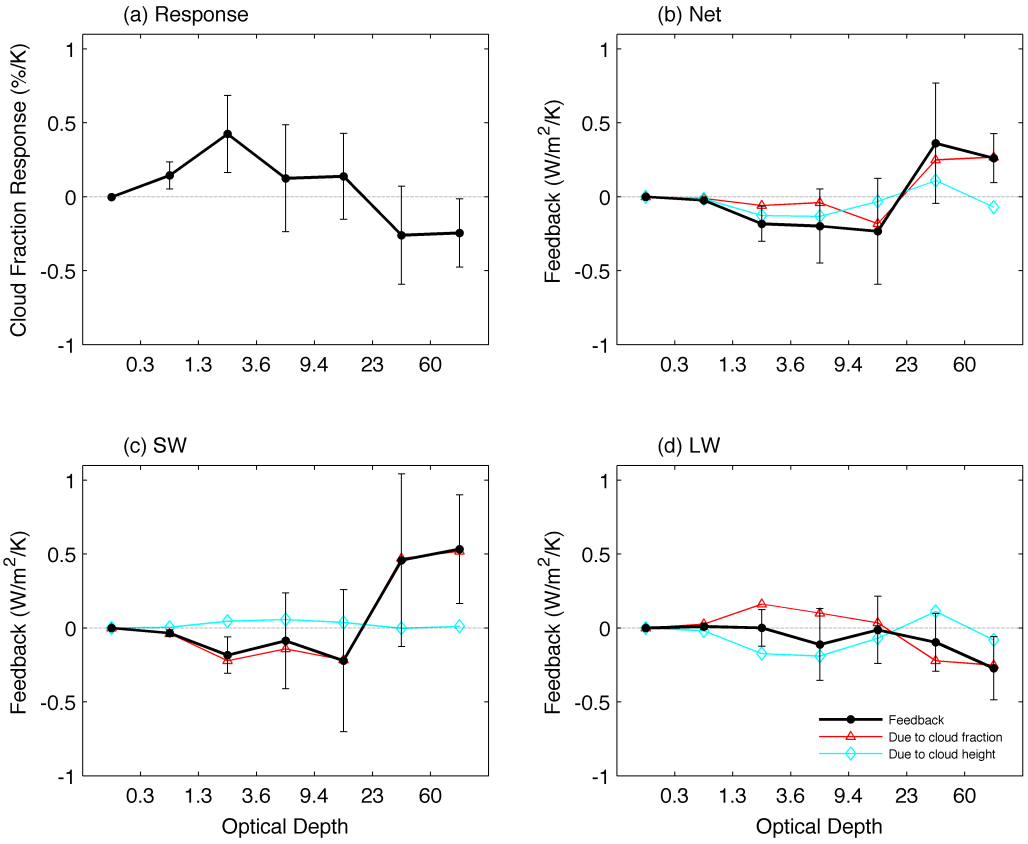

559 Figure 7. (a) Slope of the regression of cloud fraction vs. ΔT_s (%/K), as a function of cloud
560 optical depth. (b-d) The heavy line shows the contribution to the net, SW, and LW cloud
561 feedbacks, respectively. The error bars indicate the 95% confidence interval. Also shown are
562 the contributions to the cloud feedback at each optical depth from changes in cloud top height
563 and cloud fraction, holding all else fixed.

564

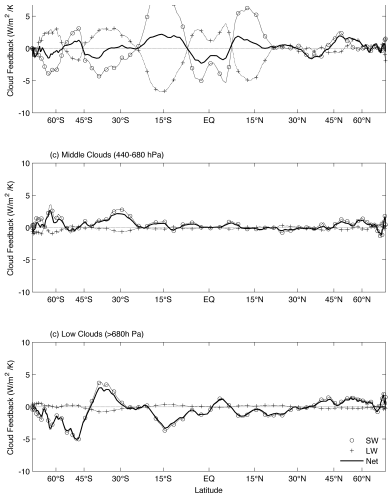

565
566 Figure 8. The zonal mean (a) high, (b) mid-level, and (c) low cloud feedbacks. The black solid
567 line is the total cloud feedback calculated from MODIS. The lines marked with circles and
568 plus signs represent the SW and LW components of the feedback, respectively.

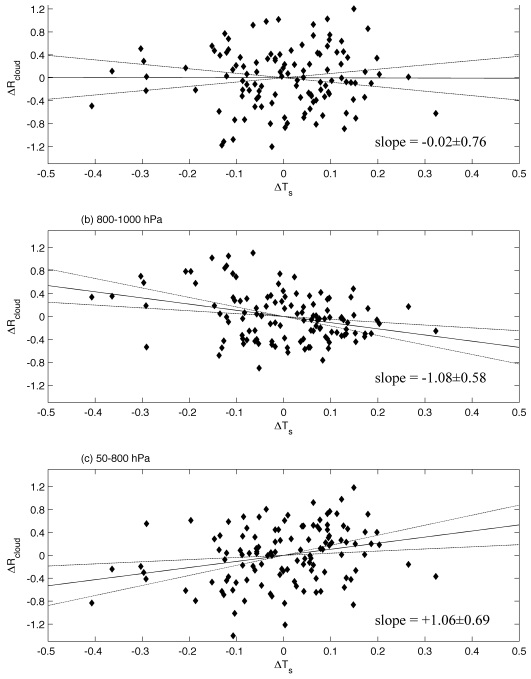

569
570 Figure 9. Scatter plot of global average ΔR_{cloud} vs. ΔT_s for (a) the entire troposphere (50-1000
571 hPa), (b) the 800-1000 hPa layer, and (c) the 50-800 hPa layer. The least-squares fit and the
572 2σ uncertainty of the fit are also plotted.